# Metadata of the chapter that will be visualized in SpringerLink

| | | |
|---|---|---|
| Book Title | Proceedings of XXVI AIMETA Conference 2024 | |
| Series Title | | |
| Chapter Title | Effects of Couple Tractions on Contact Problems at the Microscale | |
| Copyright Year | 2026 | |
| Copyright HolderName | The Author(s), under exclusive license to Springer Nature Switzerland AG | |


| | | |
|---|---|---|
| Corresponding Author | Family Name | **Radi** |
| | Particle | |
| | Given Name | **Enrico** |
| | Prefix | |
| | Suffix | |
| | Role | |
| | Division | Dipartimento Di Scienze E Metodi Dell'Ingegneria |
| | Organization | Università Di Modena E Reggio Emilia |
| | Address | Reggio Emilia, Italy |
| | Email | eradi@unimore.it |
| Author | Family Name | **Alinia** |
| | Particle | |
| | Given Name | **Yadollah** |
| | Prefix | |
| | Suffix | |
| | Role | |
| | Division | Department of Mechanical Engineering |
| | Organization | Hakim Sabzevari University |
| | Address | Sabzevar, Iran |
| | Email | yaalinia@gmail.com |
| Author | Family Name | **Güler** |
| | Particle | |
| | Given Name | **Mehmet A.** |
| | Prefix | |
| | Suffix | |
| | Role | |
| | Division | College of Engineering and Technology |
| | Organization | American University of the Middle East |
| | Address | Egaila, Kuwait |
| | Email | mehmet.guler@aum.edu.kw |



| | |
|---|---|
| Abstract | In this study, the problem of a thin film loaded at both ends and in contact with a microstructured substrate modelled by the couple stress theory of elasticity is investigated. To appropriately define the microstructural contact conditions the contribution of couple tractions is considered. By using the Green's functions for a tangential point force and a couple acting on the surface of a couple stress elastic half-plane, the extended boundary conditions, which enforce compatibility between the displacement and rotations along the contact region, provide two singular integral equations. One of them yields an explicit relation |

for couple tractions in terms of the interfacial shear stress. By assuming a series of Chebyshev polynomials for the distributions of shear stress along the contact region and using a collocation method, the remaining integral equation is reduced to an algebraic system for the Chebyshev series coefficients. Finally, the axial load in the thin film is computed while varying the characteristic length of the substrate, revealing significant deviations from the classical elastic solution.

Keywords (separated by '-') Contact mechanics - Couple stress elasticity - Thin film

# Effects of Couple Tractions on Contact Problems at the Microscale

Enrico Radi[1(✉)], Yadollah Alinia[2], and Mehmet A. Güler[3]

[1] Dipartimento Di Scienze E Metodi Dell'Ingegneria, Università Di Modena E Reggio Emilia, Reggio Emilia, Italy
eradi@unimore.it

[2] Department of Mechanical Engineering, Hakim Sabzevari University, Sabzevar, Iran

[3] College of Engineering and Technology, American University of the Middle East, Egaila, Kuwait
mehmet.guler@aum.edu.kw

**Abstract.** In this study, the problem of a thin film loaded at both ends and in contact with a microstructured substrate modelled by the couple stress theory of elasticity is investigated. To appropriately define the microstructural contact conditions the contribution of couple tractions is considered. By using the Green's functions for a tangential point force and a couple acting on the surface of a couple stress elastic half-plane, the extended boundary conditions, which enforce compatibility between the displacement and rotations along the contact region, AQ1 provide two singular integral equations. One of them yields an explicit relation for couple tractions in terms of the interfacial shear stress. By assuming a series of Chebyshev polynomials for the distributions of shear stress along the contact region and using a collocation method, the remaining integral equation is reduced AQ2 to an algebraic system for the Chebyshev series coefficients. Finally, the axial load in the thin film is computed while varying the characteristic length of the substrate, AQ3 revealing significant deviations from the classical elastic solution.

**Keywords:** Contact mechanics · Couple stress elasticity · Thin film

## 1 Introduction

Microstructured surfaces are crucial in improving the efficiency of electrolytic cells by enhancing reaction kinetics, improving mass transport, and reducing energy losses. Their increased surface area provides more sites for electrochemical reactions to occur, leading to faster reactions and higher current densities within the same geometric footprint. In proton exchange membrane (PEM) fuel cells, these surfaces also enhance the performance of catalyst layers. Additionally, the rise of additive manufacturing has brought significant attention to thin film/substrate systems in micro- and nano-electromechanical systems (MEMS/NEMS). In these applications, the characteristic length scale of the structure may become comparable to that of the material's intrinsic length, making classical elasticity theory insufficient for capturing size-dependent behavior. Atomistic simulations and lattice models can address these limitations but are computationally


M. Fraldi et al. (Eds.): AIMETA 2024, LNME, pp. 1–8, 2026.
https://doi.org/10.1007/978-3-032-17231-0_30

expensive. A more practical alternative is to use enhanced constitutive theories that allow for introducing a characteristic length, such as the couple stress elasticity (CSE) theory. According to this theory, the interaction at the microscale between the bodies in contact is described by a richer set of tractions including higher-order stress components, like couple tractions. Recently, this theory has been applied to investigate the size-dependent contact behavior of thin films on substrates. For instance, the contact problem between an Euler-Bernoulli microbeam and a CSE substrate was studied in [1], assuming the interaction occurs via couple tractions. Under this assumption, a strong size effect was observed on the internal shear forces and bending moments of the microbeam when its length is comparable to the characteristic length of the substrate. Subsequently, the study was extended in [2] to consider a receding contact between the beam and the substrate. It was found that incorporating size dependency results in highly peaked contact pressures near the load application point, and it alters the contact pressure distribution significantly when the characteristic lengths of the substrate and contact zone are comparable. Here, we present an application to the problem of a thin film loaded at both ends and bonded to a microstructured substrate subject to a uniform strain resulting from remote mechanical or thermal loading conditions.

## 2 Governing Equations

The problem of a thin film of length $2a$ and thickness $h$ perfectly bonded to a CSE substrate is shown in Fig. 1. The line loads $Q_1$ and $Q_2$ are applied to the right and left edges of the film, respectively. The interaction between the film and the substrate is modeled by the interfacial shear stress, $\tau = \tau_{yx}$, and the couple tractions, $m = m_{yz}$, distributed along the interface, namely for $-a < x < a$, while the peeling stress $\sigma_{yy}$ is neglected due to the thin film approximation [3]. The Green's functions for a tangential point force and a couple acting upon the top of the CSE half-plane are used for setting the microstructural contact conditions. The tangential displacement $u_x$ at the surface of a couple stress elastic half-plane due to a concentrated tangential load $F$ and a counterclockwise couple $C$ acting at the origin of the coordinate system was obtained in [1, 4], namely

$$u_x(x,0) = F\,\frac{1-\nu_s}{\pi\,\mu_s}\int_0^\infty \frac{\sqrt{1+s^2l^2}}{s\;g\;(sl)}\,\cos sx\;ds - C\,\frac{1-\nu_s}{\pi\,\mu_s}\int_0^\infty \frac{\sqrt{1+s^2l^2}-sl}{g\;(sl)}\,\cos sx\;ds, \tag{1}$$

where $\mu_s$, $\nu_s$, and $l$ are the elastic shear modulus, the Poisson's ratio, and the characteristic length of the CSE substrate, respectively, and

$$g(z) = \sqrt{1+z^2} + 4(1-\nu_s)z^2(\sqrt{1+z^2}-z). \tag{2}$$

The corresponding axial strain along the half-plane surface then follows from the derivative of the displacement (1) with respect to the variable $x$ as

$$\varepsilon^s_{xx}(x,0) = -F\,\frac{1-\nu_s}{\pi\,\mu_s}\int_0^\infty \frac{\sqrt{1+s^2l^2}}{g\;(sl)}\,\sin sx\;ds + C\,\frac{1-\nu_s}{\pi\,\mu_s}\int_0^\infty \frac{\sqrt{1+s^2l^2}-sl}{g\;(sl)}\,s\sin sx\;ds. \tag{3}$$

The balance equations for the thin film require (Fig. 1)

$$\tau(x) = N'(x), \qquad m(x) = -\mathrm{t}(x)h/2 \tag{4}$$

where $\tau(x)$ and $m(x)$ are the shear tractions and couple tractions exchanged between the thin film and the couple stress substrate, $N$ is the axial load in the thin film and the prime denotes the derivative with respect to $x$. Let us now consider a thin film of length $2a$ and thickness $h << a$ perfectly bonded to the couple stress substrate (Fig. 1), under plane strain conditions. The axial load in the thin film and the corresponding axial strain follow from the integration of eqn $(4)_1$ between $-a$ and $x$, using the boundary conditions $N(-a) = Q_2$:

$$N(x) = Q_2 + \int_{-a}^{x} \tau(t)\, dt, \qquad \varepsilon^f_{xx}(x) = \frac{1-\nu_f^2}{E_f h} N(x) = \frac{1-\nu_f^2}{E_f h}\left[Q_2 + \int_{-a}^{x} \tau(t)\, dt\right], \tag{5}$$

where $E_f$ and $\nu_f$ are the elastic Young modulus and the Poisson's ratio of the elastic thin film, respectively. For the whole film one has $N(a) = Q_1$. By using the Green's function (3), the surface strain on the top of the substrate loaded by the shear and couple tractions, $\tau(x)$ and $m(x)$ as sketched in Fig. 1, is given by

$$\varepsilon^s_{xx}(x,0) = -\frac{1-\nu_s}{\pi\,\mu_s}\left\{\int_{-a}^{a} \tau(t)\,dt \int_0^{\infty} \frac{\sqrt{1+s^2l^2}}{g(sl)} \sin[s\,(x-t)]\,ds - \int_{-a}^{a} m(t)dt \int_0^{\infty} \frac{\sqrt{1+s^2l^2}-sl}{g(sl)}\, s\sin[s\,(x-t)]\,ds\right\} + \varepsilon^0_{xx}, \tag{6}$$

where $\varepsilon^0_{xx}$ is the thermal strain of the substrate. The strain compatibility condition between the film and the substrate then requires: $\varepsilon^s_{xx}(x,0) = \varepsilon^f_{xx}(x),$ , namely, by using Eqs. $(5)_2$, (6), and the balance condition $(4)_2$:

$$\frac{\lambda}{2h}\left[Q_2 + \int_{-a}^{x} \tau(t)\,dt\right] = -\frac{1}{2\pi}\int_{-a}^{a} \tau(t)\,dt \int_0^{\infty} \frac{2\sqrt{1+s^2l^2} + (\sqrt{1+s^2l^2}-sl)\,sh}{g(sl)} \sin[s\,(x-t)]\,ds + \frac{\mu_s\varepsilon^0_{xx}}{1-\nu_s}, \tag{7}$$

where $\lambda = \mu_s\,(1-\nu_f\,)/[\mu_s(1-\nu_s)\,]$ is the relative stiffness ratio. By performing an asymptotic expansion of the kernel function as $s \to \infty$ to single out the most singular terms, as in [3], and introducing the non-dimensional quantities: $H = h/a$, $\Lambda = l/a$, $z = sa$, $\xi = x/a$, $\eta = t/a$, and $\rho = Q_2/Q_1$, then, the integral equation (7) becomes

$$\frac{\lambda}{2H}\int_{-1}^{\xi} \tau(\eta)\,d\eta + \int_{-1}^{1} \kappa(\xi-\eta)\tau(\eta)\,d\eta + \frac{1}{3-2\nu_s}\left\{\frac{1}{\pi}\int_{-1}^{1} \frac{\tau(\eta)}{\xi-\eta}d\eta + \frac{H}{8\Lambda^2}\left[\int_{-1}^{\xi} \tau(\eta)d\eta - \int_{\xi}^{1} \tau(\eta)d\eta\right]\right\} = \frac{\mu_s\varepsilon^0_{xx}}{1-\nu_s} - \frac{\lambda\rho\,Q_1}{2Ha}, \tag{8}$$

where

$$\kappa(\xi) = \frac{1}{2\pi\,(3-2\nu_s)}\int_0^{\infty}\left[4(1-\nu_s) - \frac{H}{2\Lambda^2 z}\right]\frac{(1-2\Lambda^2z^2)\sqrt{1+\Lambda^2z^2}+2\Lambda^3z^3}{g(z\Lambda)}\sin z\xi\, dz. \tag{9}$$

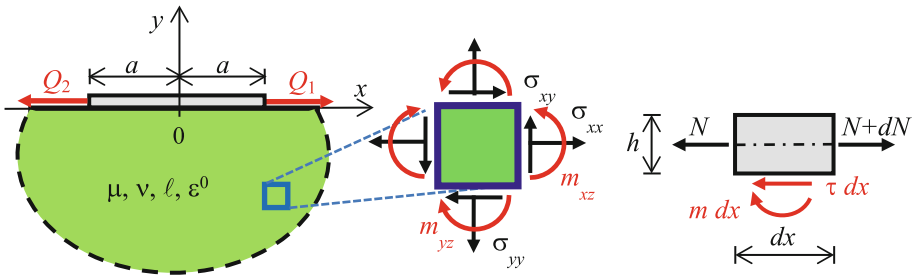


**Fig. 1.** Thin film attached to a CSE substrate loaded by line loads $Q_1$ *and* $Q_2$, *and free body diagram of forces and couples acting on any infinitesimal thin film element of thickness h.*

## 2.1 Collocation Procedure

At the edges of the contact $x = \pm a$ , the shear stress τ must display square root singularity. According to Eq. $(4)_2$, the couple tractions $m$ also displays square root singularity at $\xi = \pm a$. Therefore, we represent the shear stress by using a truncated series of Chebyshev polynomials of the first kind $T_n$, as in [3–6] and [7]:

$$\tau(\eta) = \frac{Q_1}{a} \sum_{n=0}^{K} c_n \frac{T_n(\eta)}{\sqrt{1-\eta^2}}, \qquad for\ |\eta| \le 1. \tag{10}$$

Then, from the balance condition for the thin film, $N(a) = Q_1$, one obtains $c_0 = (1–\rho)/\pi$. The unknown coefficients $c_n$ ($n = 1, 2,\ldots, K$) can be calculated by using a collocation procedure, namely by solving a linear system of $K$ algebraic equations obtained from the governing integral Eq. (8) evaluated at $K$ collocation points $\xi_k$ ($k = 1, 2, ..., K$), which are taken as the roots of the Chebyshev polynomial $T_{2K}(\xi)$, namely

$$\sum_{n=1}^{K} c_n \left\{ \frac{2\pi}{M} \sum_{j=1}^{M} \kappa(\xi_k - \eta_j) T_n(\eta_j) - \left[ \frac{2}{3-2\nu_s} + \left( \frac{H}{(6-4\nu_s)\,\Lambda^2} + \frac{\lambda}{H} \right) \frac{\sqrt{1-\xi_k^2}}{n} \right] U_{n-1}(\xi_k) \right\}$$
$$+ (1-\rho) \left[ \frac{2}{M} \sum_{j=1}^{M} \kappa(\xi_k - \eta_j) + \left( \frac{H}{(6-4\nu_s)\Lambda^2} + \frac{\lambda}{H} \right) \left( \frac{1}{2} - \frac{\arccos \xi_k}{\pi} \right) \right] = 2\gamma - \frac{\lambda\,(1+\rho)}{2H}, \tag{11}$$

where

$$\gamma = \frac{a\,\mu_s \varepsilon_{xx}^0}{(1-\nu_s)\,Q_1}, \quad \xi_k = \cos\frac{(2k-1)\,\pi}{2K}, \quad \eta_j = \cos\frac{(2j-1)\,\pi}{2M}, \tag{12}$$

for $k = 1, 2, \ldots, K$, and $j = 1, 2, \ldots, M$. Note that the definite integral in Eq. (8) containing the kernel function $\kappa$ ($\xi - \eta$) has been calculated in Eq. (11) by using the Gauss-Chebyshev quadrature with $M$ nodes $\eta_j$ ($j = 1, 2, \ldots, M$) coinciding with the roots of the Chebyshev polynomial $T_M(\eta)$ defined in $(12)_3$. Once all the coefficients $c_n$, for $n = 0, 2, \ldots, K$, are calculated, the interfacial shear stress is given by (10) and the axial load in the thin film follows from Eqs. (5) and (10) as

$$N(\xi) = Q_2 + Q_1 \sum_{n=0}^{K} c_n \int_{-1}^{\xi} \frac{T_n(\eta)}{\sqrt{1-\eta^2}}\, d\eta = \left[ \rho + (1-\rho) \left( 1 - \frac{\arccos \xi}{\pi} \right) - \sum_{n=1}^{\infty} \frac{c_n}{2n} U_{n-1}(\xi) \sqrt{1-\xi^2} \right] Q_1. \tag{13}$$

The strength of the shear stress singularity in the CSE substrate at the right and left film edges, $k_1$ and $k_2$, are defined by

$$k_1 = \lim_{x \to a} \sqrt{2(a-x)}\, \tau(x), \qquad k_2 = \lim_{x \to -a} \sqrt{2(a+x)}\, \tau(x), \tag{14}$$

respectively. By introducing the shear stress representation (10), they become:

$$k_1 = \frac{Q_1}{a} \sum_{n=0}^{K} c_n, \qquad k_2 = \frac{Q_1}{a} \sum_{n=0}^{K} (-1)^n c_n. \tag{15}$$

## 3 Results

In the following, a Poisson's ratio $\nu_s = 0.3$ is assumed both for the film and substrate, and a number $N \geq 50$ of terms is taken in the Chebyshev series expansion (10). Two special loading case are considered, namely symmetric loading for $\rho = 1$ ($Q_1 = Q_2 = Q$). And skew-symmetric loading for $\rho = -1$ ($Q_1 = -Q_2 = Q$) and $\gamma = 0$. The case of $\rho = 0$ and $\gamma = 0$ can be found in [3]. Note that the shear stress distribution becomes skew-symmetric under symmetric loading and thus only odd terms are considered in the series expansion (10), vice versa the shear stress distribution is symmetric under skew-symmetric loading, so that only even terms are considered.

The effects of the size parameter, $l/a$, both on the normalized shear stress distribution along the contact zone, $\tau\, a/Q$, and the axial load in the thin film, $N/Q$, are illustrated in Fig. 2 under two equal symmetric line loads $Q$ applied at the film edges, for $a/h = 30$ and $\lambda = 1/3$. The shear stress distribution for classical elastic behavior of the substrate obtained from the approach presented in [5] is also reported in Fig. 2 (black dashed line). As expected, the shear stress distribution attains the largest value near the loaded edges of the film, where it displays square root singularity. Introducing the size effect, namely increasing the ratio $l/a$, the axial load is transferred to the CSE substrate at a smaller distance to the loaded edges. No significant changes are observed in the shear stress and axial load in the film for $l/a > 0.5$. Moreover, the results approach the classical elastic solution [5] for a small but finite value of the characteristic length, thus validating the present approach.

The effects of the substrate strain due to mechanical or thermal loading are considered in Fig. 3 for $\gamma = 1$, and for different values of the characteristic length ratio $l/a$. In this case, the shear stress distribution is similar to that obtained for $\gamma = 0$ in Fig. 2, and the axial load in the thin film is a bit larger due to the contribution of the substrate strain.

The normalized shear stress distribution, $\tau\, a/Q$, and axial load, $N/Q$, under two skew-symmetric line loads $Q$ applied at the film edges, are plotted in Fig. 4, for $a/h = 30$, $\lambda = 1/15$ and for various characteristic length ratios $l/a$. The classic elastic solution obtained from [5] is also plotted (black dashed lines). The shear stress distribution is symmetric and displays square root singularity near the loaded edges of the film. As the ratio $l/a$ increases, the shear stress decreases in the central part of the film and the axial load is transferred to the CSE substrate at a smaller distance to the loaded edges. No significant changes are observed for $l/a > 0.5$. The classical elastic solution is recovered for a small

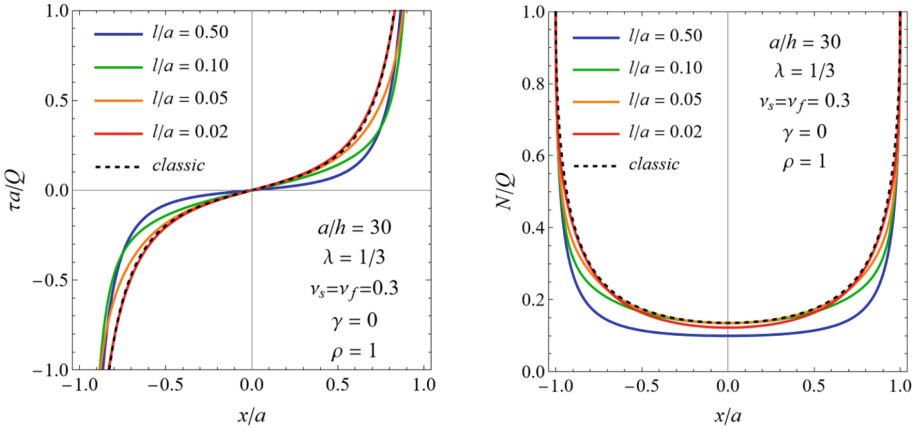


**Fig. 2.** Normalized distributions of the interfacial shear stress and axial load in the thin film for various values of the ratio l/a under symmetric loading ($Q_1 = Q_2 = Q$).

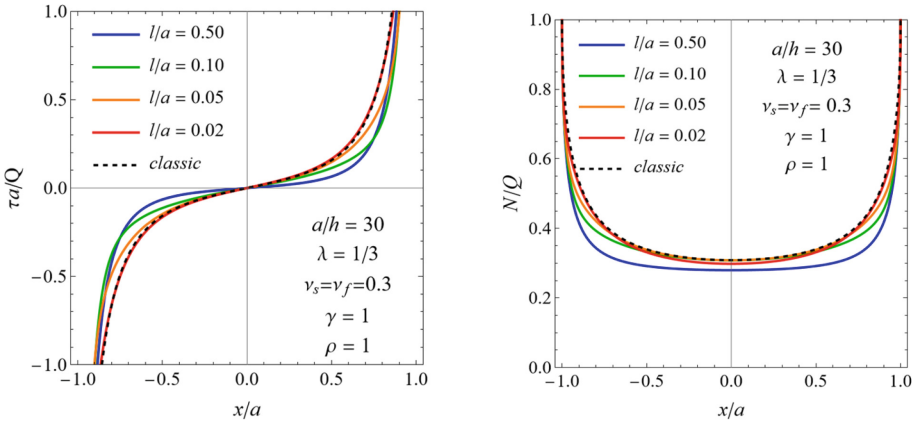


**Fig. 3.** Normalized distributions of the interfacial shear stress and axial load in the thin film for various values of the ratio l/a under symmetric loading and substrate strain.

but finite value of the ratio $l/a$. Indeed, for $l = 0$ the couple tractions also vanish along the interface, then for a finite film thickness $h > 0$ the balance condition $(4)_2$ cannot be satisfied for $\tau\ (x) \neq 0$ if the bending stiffness of the film is neglected.

Finally, the variations of the strength of stress singularity are presented in Fig. 5 for $a/h = 30$ and $\lambda = 1/15$, by varying the characteristic length, both for symmetric and skew-symmetric loading conditions. The strength of stress singularity is almost unaffected by the characteristic length of the material under symmetric loading, whereas it significantly increases with the characteristic length under skew-symmetric loading, and it attains an almost constant value for $l/a > 0.2$.

According to [5], the normalized strength of stress singularity $k_1 a/Q$ for classical elastic behavior of the substrate with $a/h = 30$ and $\lambda = 1/15$, is equal to 0.648 under

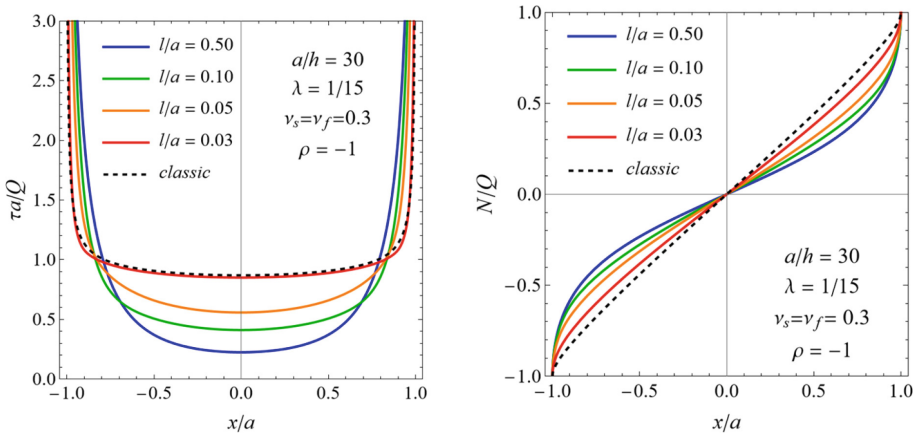


**Fig. 4.** Normalized distributions of the interfacial shear stress and axial load in the thin film for various values of the ratio l/a under skew symmetric loading ($Q_1 = -Q_2 = Q$).

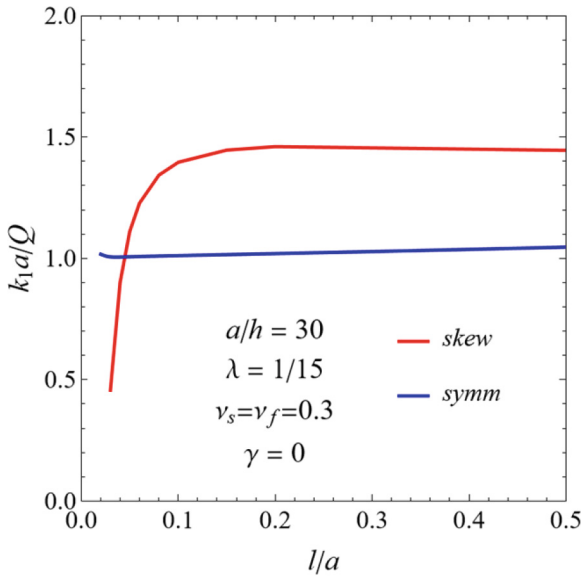


**Fig. 5.** Normalized variations of the strength of stress singularities $k_1$ *with the characteristic length ratio l/a under symmetric and skew symmetric loading.*

symmetric loading and to 0.291 under skew-symmetric loading. Therefore, accounting for the substrate microstructures yields a significant increase in the strength of stress singularity at the film edges.

## 4 Conclusions

This work presents an analytical model based on Chebyshev series expansions to investigate the contact problem between a thin elastic film under tension and a CSE substrate. The most important features of the present study are:

- the capability to calculate shear and couple tractions along the interface, the axial stress at any point in the thin film, and the strength of stress singularity at the film ends under general loading;
- the use of Chebyshev series expansions for solving a singular integral equation instead of purely numerical procedures;
- the parametric nature of the analysis and the possibility of using it for any geometry and constitutive parameters of the film and the substrate;
- the capability of the model to account for the film thickness in the balance equation of the film.

The present work demonstrates that accounting for non-classical and size-dependent behavior of the substrate as well as for couple tractions yields a remarkable reduction of the axial load and axial stress within the thin film. Moreover, the results provided by the present model prove that the couple tractions significantly contribute to the contact interaction, and they have to be considered in the modeling of contact problems if the substrate is micropolar and size dependent.

**Acknowledgements.** The authors are grateful to the Italian "Gruppo Nazionale di Fisica Matematica" (INdAM-GNFM) for financial supporting the visiting professor M.A. Güler.

## References

1. Radi, E.: A loaded beam in full frictionless contact with a couple stress elastic half-plane: Effects of non-standard contact conditions. Int. J. Solids Struct. **232**, 111175 (2021)
2. Radi, E., Nobili, A., Güler, M.A.: Indentation of a free beam resting on an elastic substrate with an internal lengthscale. Eur. J. Mech.-A/Solids **10**, 104804 (2022)
3. Güler, M.A., Alinia, Y., Radi, E.: Couple stress effects in a thin film bonded to a half-space. Math. Mech. Solids **29**, 629–644 (2024)
4. Song, H.X., Ke, L.L., Wang, Y.S.: Sliding frictional contact analysis of an elastic solid with couple stresses. Int. J. Mech. Sci. **133**, 804–816 (2017)
5. Erdogan, F., Gupta, G.D.: The problem of an elastic stiffener bonded to a half plane. J. Appl. Mech. **38**, 937–941 (1971)
6. Abbaszadeh-Fathabadi, S.A., Alinia, Y., Güler, M.A.: On the mechanics of a double thin film on a finite thickness substrate. Int. J. Solids Struct. **279**, 112349 (2023)
7. Guler, M.A., Gülver, Y. F., Nart, E.: Contact analysis of thin films bonded to graded coatings. Int. J Mech. Sci. **55**, 50–64 (2012)

# Author Queries

**Chapter 30**

| Query Refs. | Details Required | Author's response |
|---|---|---|
| AQ1 | Please check and confirm if the authors Given and Family names have been correctly identified. | |
| AQ2 | This is to inform you that corresponding author has been identified as per the information available in the Copyright form. | |
| AQ3 | As Per Springer style, both city and country names must be present in the affiliations. Accordingly, we have inserted the city and country names in the affiliation. Please check and confirm if the inserted city and country names are correct. If not, please provide us with the correct city and country names. | |

**Alternative Texts for Your Images, Please Check and Correct them if Required**

| Page no | Fig/Photo | Thumbnail | Alt-text Description |
|---|---|---|---|
| 4 | Fig1 | 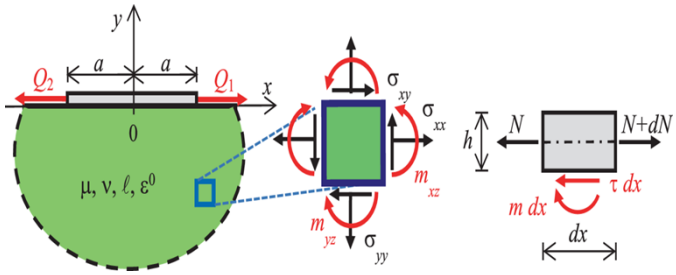 | Diagram illustrating a mechanical system with three main components. On the left, a semicircular green shape with labeled parameters: \( \mu, \nu, \ell, \varepsilon^0 \), and forces \( Q_1 \) and \( Q_2 \) acting horizontally. In the center, a magnified square section shows stress components \( \sigma_{xx}, \sigma_{yy}, \sigma_{xy} \) and moments \( m_{xz}, m_{yz} \) with arrows indicating directions. On the right, a rectangular element with height \( h \) and width \( dx \) shows forces \( N \) and \( N + dN \), and shear stress \( \tau \) with moment \( m \). Arrows indicate force and moment directions. |
| 6 | Fig2 | 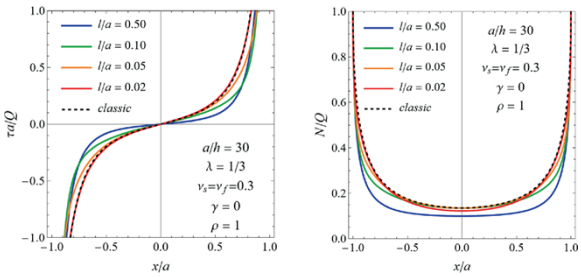 | Two-panel figure showing X-Y charts. **Left Panel:** The chart plots \(\tau a/Q\) against \(x/a\) with curves for different \(l/a\) values: 0.50 (blue), 0.10 (green), 0.05 (orange), and 0.02 (red). A dashed line represents the "classic" model. Parameters include \(a/h = 30\), \(\lambda = 1/3\), \(v_s = v_f = 0.3\), \(\gamma = 0\), and \(\rho = 1\). **Right Panel:** The chart plots \(N/Q\) against \(x/a\) with similar color coding for \(l/a\) values and a dashed "classic" line. Parameters are \(a/h = 30\), \(\lambda = 1/3\), \(v_s = v_f = 0.3\), \(\gamma = 0\), and \(\rho = 1\). |

| Page no | Fig/Photo | Thumbnail | Alt-text Description |
|---|---|---|---|
| 6 | Fig3 | 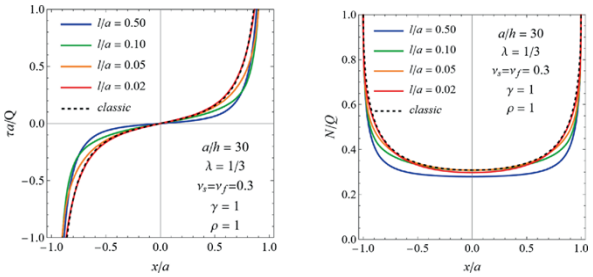 | Two X-Y charts are displayed side by side. The left chart plots \(\tau a/Q\) against \(x/a\), showing curves for different values of \(l/a\) (0.50, 0.10, 0.05, 0.02) and a classic model. The right chart plots \(N/Q\) against \(x/a\) with similar parameters. Both charts include annotations: \(a/h = 30\), \(\lambda = 1/\beta\), \(v_s = v_f = 0.3\), \(\gamma = 1\), and \(\rho = 1\). The curves are color-coded and labeled accordingly. |
| 7 | Fig4 | 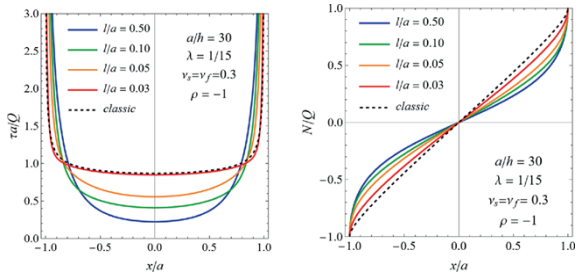 | Two-panel figure showing X-Y charts. The left panel plots \(\tau a/Q\) against \(x/a\) with curves for different \(l/a\) values: 0.50 (blue), 0.10 (green), 0.05 (orange), and 0.03 (red), compared to a classic model (dashed black line). The right panel plots \(N/Q\) against \(x/a\) with the same color scheme and classic model comparison. Both panels include parameters: \(a/h = 30\), \(\lambda = 1/15\), \(v_s = v_f = 0.3\), and \(\rho = -1\). |
| 7 | Fig5 | 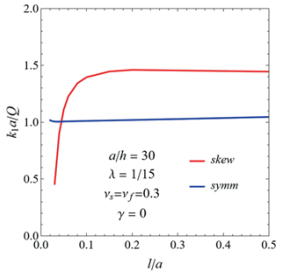 | Graph showing the relationship between \( l/a \) on the x-axis and \( k_1 a/Q \) on the y-axis. Two lines are plotted: a red line labeled "skew" and a blue line labeled "symm." The red line rises sharply before leveling off, while the blue line remains relatively constant. Annotations include \( a/h = 30 \), \( \lambda = 1/15 \), \( \nu_s = \nu_f = 0.3 \), and \( \gamma = 0 \). |